Abstract

LI, ZHENGMIN. Molecular Dynamics Simulations of Micellization in Model Surfactant / CO_2 Systems. (Under the direction of Carol K. Hall)

Discontinuous molecular dynamics simulations are performed on surfactant (H_nT_m) / solvent systems modeled as a mixture of single-sphere solvent molecules and freely-jointed surfactant chains composed of n slightly solvent-philic head spheres (H) and m solvent-philic tail spheres (T), all of the same size. We use a square-well potential to account for the head-head, head-solvent, tail-tail and tail-solvent interactions and a hard sphere potential for the head-tail and solvent-solvent interactions. We first simulate homopolymer / supercritical CO_2 ($scCO_2$) systems to establish the appropriate interaction parameters for a surfactant / $scCO_2$ system. Next we simulate surfactant / $scCO_2$ systems and explore the effect of the surfactant mole fraction, packing fraction and temperature on the phase behavior of a surfactant / $scCO_2$ system. The transition from the two-phase region to the one-phase region is located by monitoring the contrast structure factor of the equilibrated surfactant / $scCO_2$ system and the micelle to unimer transition is located by monitoring the micelle size distribution of the equilibrated surfactant / $scCO_2$ system. The phase diagram for the surfactant / $scCO_2$ system and the density dependence of the critical micelle concentration are in qualitative agreement with experimental observations. The phase behavior of a surfactant / $scCO_2$ system can be directly related to the solubilities of the corresponding homopolymers that serve as the head and tail block for the surfactant. The location of the micelle-unimer transition is strongly affected by the head-solvent attraction but only weakly affected by the tail-tail and tail-solvent attrac-

tions. Both micellization and phase separation upon decreasing the temperature are found in our simulations.

Molecular Dynamics Simulations of Micellization in Model Surfactant / CO_2 Systems

by

Zhengmin Li

A thesis submitted to the Graduate Faculty
of North Carolina State University
in partial fulfillment of the
requirements for the Degree of
Master of Science

Chemical Engineering

Raleigh, NC 27695

2003

APPROVED BY:

Carol K. Hall
Chair of Advisory Committee

Peter K. Kilpatrick

John H. van Zanten

Biography

The author was born in Leping, Jiangxi Province, P. R. China on September 1, 1971. She is the second daughter of Yiwen and Yueying Li and has one elder sister, Zhenggang, one younger sister, Guohong, and one younger brother, Zhengwei. She received a B.S. degree in Chemical Engineering from Tianjin University at Tianjin, P. R. China in July, 1993 and a M.S. degree in Chemical Engineering from Tsinghua University at Beijing, P. R. China in July, 1999. On December 17, 1997, she married Jian Xu of Leping, Jiangxi Province, P. R. China. In August, 1999, she was admitted to North Carolina State University to pursue graduate studies in Chemical Engineering.

Acknowledgement

It is my pleasure to acknowledge the people who have contributed to the preparation of this thesis by supporting and encouraging me.

First, I would like to thank my advisor, Professor Carol Hall, for her guidance and patience in both academic and personal matters. Professor Hall is devoted to advising her graduate students and I am grateful to be one of her students.

I thank the STC program of the National Science Foundation for funding under agreement No. CHE-9876674. Acknowledgment is made to the Office of Energy Research, Basic Sciences, Chemical Science Division of the U. S. Department of Energy and the Donors of the Petroleum Research Fund administered by the American Chemical Society for partial support of this work.

To the members of the Hall research group, past and present, I thank you for your friendship and encouragement. I would like thank Brian Attwood and Andrew Schultz for keeping the computers running smoothly. I feel especially indebted to Andrew Schultz as he has spent so much time discussing my research and explaining the simulation techniques.

To my family, especially my parents, I thank you for the love and encouragement that support my study abroad. Finally I thank my husband, Jian, for supporting me and making me happy in the past years.

Contents

List of Figures

1 Introduction

Supercritical carbon dioxide ($scCO_2$) has received a great deal of scientific and industrial attention as a potential alternative to organic solvents because it is environmentally benign[1] and the temperature and pressure ranges for its operation are easily accessible ($T_c = 31^oC$, $P_c = 73.8$ bar). An additional attractive feature of $scCO_2$ as a solvent is that solute solubility can be controlled by varying pressure as well as temperature due to $scCO_2$'s high compressibility. However, since few substances (except for flurorinated polymers and silicones) can be readily dissolved in $scCO_2$,[2–7] surfactants are necessary to assist the solvation process. During the last decade, a great deal of experimental effort has been devoted to the study of surfactants in $scCO_2$.[8–14] In comparison, there have been relatively few attempts to use molecularly-based theory or computer simulation to understand the solvation of surfactants in $scCO_2$.[15–19] The long-term goal of this study is to gain enough insight into how surfactant intermolecular forces and geometry affect the performance of surfactants in $scCO_2$ to provide a useful set of guidelines for the design of new surfactants for specific applications in $scCO_2$.

Buhler et al. used static and dynamic light scattering to explore the effect of varying the CO_2 density on the phase behavior of surfactant polyvinyl acetate - b - poly(1,1,2,2 - tetrahydroperfluorooctyl acrylate) (PVAc-b-PTAN) in supercritical CO_2 while maintaining the temperature and the surfactant / $scCO_2$ molar ratio fixed.[14] They observed three different regions in the phase diagram when plotted in the surfactant concentration $-$ $scCO_2$ density plane: a two-phase region at low CO_2 densities, spherical micelles at intermediate densities, and a unimer solution at high densities. This was the first observation that a transition from micelles to

unimers could be induced by increasing CO_2 density. They also found that the solubilities of both PVAc and PTAN homopolymers in $scCO_2$ increase as $scCO_2$ density increases. They interpreted the transition from micelles to unimers (micelle $\rightarrow$ unimer transition) upon increasing the solvent density as a result of an increase in solvent quality for both surfactant blocks. The $scCO_2$ density at which the micelle $\rightarrow$ unimer transition occurs is called the critical micelle density (CMD)[13]. The micelle $\rightarrow$ unimer transition line on the phase diagram as plotted in the surfactant concentration$-CO_2$ density plane is referred to as the CMD when viewed at fixed surfactant concentration and as the critical micelle concentration (CMC) when viewed at fixed CO_2 density. Buhler et al.[14] found that the CMC increases as the $scCO_2$ density increases, which means that more surfactant molecules can be dissolved at high $scCO_2$ densities than at low $scCO_2$ densities.

There have been numerous simulation studies of incompressible model surfacant systems using highly simplified models over the years.[20–27] Quite recently Panagiotopoulos et al.[27] investigated the phase behavior of incompressible systems containing diblock and/or triblock surfactants in water using histogram-reweighting grand-canonical lattice Monte Carlo simulations[26]. The interactions were chosen to be short-ranged and temperature-independent for the systems they studied. The only interaction considered was the tail-tail (the tail is the solvent-phobic block) attraction. The other interactions, head-head (the head is the solvent-philic block), head-tail, head-solvent, tail-solvent and solvent-solvent were all neglected. The surfactant volume fraction at which the unimer-micelle transition occurs, $\phi_{\rm cmc}$, was found by calculating the osmotic pressure at different surfactant volume fractions.[26] They distinguished between micellization and phase separation by determining whether or not the resulting phase

diagram depended on system size. The surfactant / solvent system displayed either phase separation or micellization in the simulations depending upon the surfactant head/tail ratios, but never both; in contrast, both phase separation and micellization are observed in experiments[28]. Panagiotopoulos et al. attributed the disagreement between their simulation results and experiments to the lack of temperature-dependence in the model interactions between the surfactant molecules and water; temperature dependence was thought to be necessary to reflect the unusual solvation properties of water. They also found that ϕ_{cmc} increases as the temperature increases.

Recently there have been studies of compressible surfactant / $scCO_2$ systems using lattice Monte Carlo simulations. Lisal et al.[18] explored the self-assembly of surfactants in $scCO_2$ by introducing vacancies into Larson's lattice model[20], making the solvent density adjustable and hence the surfactant / solvent system compressible. They performed large-scale canonical Monte Carlo simulations on model surfactant [$F(CF_2)_n(CH_2CH_2O)_mH$] / $scCO_2$ systems to investigate the influence of surfactant structure (head and tail lengths), solvent density and surfactant concentration on the CMC, the micelle size distribution, and micelle size and shape. Pseudophase diagrams were constructed based on their simulation results and compared with those from experiments on surfactant [PVAc-*b*-PTAN] / $scCO_2$[14]. The simulation phase diagram was relatively consistent with experimental results except that the CMC decreased as density increased, in contrast with experimental observations that the CMC increases with increasing density. The discrepancy between the simulations and experimental results was traced to the decrease in the solubility of the CO_2-phobic block in their simulations as CO_2 density increased. As indicated above, the solubilities of both surfactant blocks (CO_2-philic

PTAN and less CO_2-philic PVAc) in the experiments of Buhler et al.[14] increased as solvent density increased.

Atomistic-level molecular dynamics simulation studies on compressible surfactant / $scCO_2$ systems have also been conducted.[16, 17, 29, 30] These studies focus on the structures formed in surfactant / $scCO_2$ systems and their dynamic properties. Salaniwal et al.[16, 17] performed molecular dynamics simulations on a dichain surfactant / $scCO_2$ system using detailed molecular models for the surfactant, [(C_7F_{15}) (C_7F_{15}) $CHSO_4^-Na^+$], and for CO_2. They studied the formation dynamics and structural properties of the reverse micelles formed by the surfactants in CO_2, obtaining results that agree qualitatively with data from scattering studies on the same dichain hydrocarbon-fluorocarbon surfactant[31]. The studies of compressible surfactant / solvent systems discussed thus far demonstrate the potential of computer simulations to provide a fundamentally-based understanding of the behavior of surfactant / supercritical fluid systems.

In this paper, we describe discontinuous molecular dynamics (DMD) simulations on surfactant (H_nT_m) / solvent systems modeled as a mixture of single-sphere solvent molecules and freely-jointed surfactant chains composed of n slightly solvent-philic head spheres (H) and m more solvent-philic tail spheres (T), all of the same size. We first simulate homopolymer (P_n) / $scCO_2$ systems of chain length $n = 4$ and 8 to help establish the appropriate interaction parameter set for a surfactant / solvent system. Parameters were chosen to ensure that the packing fraction at which the micelle $\rightarrow$ unimer transition occurs is in the desired range of $0.2 - 0.5$, which keeps the solvent density of our model systems near or above the critical density of CO_2. We perform simulations on model surfactant (H_4T_8) / $scCO_2$ systems choosing the head-head , head-solvent, tail-tail and tail-solvent attraction strengths to be 1.0, 0.5, 0.1

and 1.0, respectively, and the head-tail and solvent-solvent attractions to be zero. We explore the effect of variations in the surfactant mole fraction, packing fraction and temperature on the phase behavior, plotting slices of the phase diagram in the surfactant mole fraction−packing fraction−temperature space. We perform a sensitivity analysis for the strengths of the head-solvent, tail-tail and tail-solvent attractions so as to rank the importance of the various parameters in determining the location of the micelle → unimer transition. Finally we investigate the influence of the variation in the surfactant head/tail ratio and overall chain length on the location of the micelle → unimer transition.

Highlights of our simulation results are the following. Homopolymer solubility increases as the packing fraction, temperature and polymer-solvent attraction increase, decreases as the chain length and polymer-polymer attraction increases, in qualitative agreement with experimental results on the effect of $scCO_2$ density[14], homopolymer chain length[14, 32, 33] on homopolymer solubility in $scCO_2$. The phase diagram constructed for surfactant / solvent systems plotting in slices of the surfactant mole fraction − packing fraction − temperature space displays three regions: a two-phase region at low packing fraction and low temperature, a micelle phase at intermediate packing fraction and intermediate temperature, and a unimer phase at high packing fraction and high temperature. The packing fractions at which the two phase → one phase transition and the micelle → unimer transition occur increase as the surfactant mole fraction increases. The packing fraction at which the two phase → one phase transition of the surfactant (H_4T_8) / solvent system occurs is higher than that of a homopolymer (P_8) / solvent system when P_8 is comprised of tail beads (T), and the packing fraction at which the micelle → unimer transition of the H_4T_8 / solvent system occurs is lower than that at which the aggregate

$\rightarrow$ unimer transition of a homopolymer (P_4) / solvent system occurs when P_4 is comprised of head beads (H). The location of the micelle $\rightarrow$ unimer transition is strongly dependent on the strength of the head-solvent attraction but only weakly dependent on the strength of the tail-tail and tail-solvent attractions. The packing fraction at which the micelle $\rightarrow$ unimer transition occurs increases as the surfactant head/tail ratio increases at fixed chain length and increases as the surfactant chain length increases at fixed head/tail ratio. The surfactant solubility increases as the temperature increases at fixed packing fraction. The packing fraction at which the two phase $\rightarrow$ one phase transition or the micelle $\rightarrow$ unimer transition occurs decreases as the temperature increases.

The remainder of this paper is organized as follows: Section 2 decribes the molecular model, simulation method and methods for locating the two phase $\rightarrow$ one phase transition for homopolymer / solvent systems or surfactant / solvent systems, the micelle $\rightarrow$ unimer transition for surfactant / solvent systems and the aggregate $\rightarrow$ unimer transition for homopolymer / surfactant systems. Section 3 describes our simulation results in detail. A brief summary and discussion of our results are given in Section 4.

2 Molecular Models and Simulation Methods

The surfactant / solvent system is modeled as a mixture of single-sphere solvent molecules (S) and freely-jointed surfactant chains (H_nT_m) composed of n slightly-solvent-philic head spheres (H) and m solvent-philic tail spheres (T), all of the same size. We choose a hard-sphere potential for the solvent-solvent and head-tail interactions and a square-well potential

for the head-head, head-solvent, tail-tail and tail-solvent interactions. The hard sphere ($U_{\rm hs}$) and square-well ($U_{\rm sw}$) potentials are:

$$U_{\rm hs}(r) = \begin{cases} \infty & \text{if } r < \sigma \\ 0 & \text{if } r > \sigma \end{cases} \tag{1}$$

$$U_{\rm sw}(r) = \begin{cases} \infty & \text{if } r < \sigma \\ \epsilon & \text{if } \sigma < r < (1+\lambda)\sigma \\ 0 & \text{if } r > (1+\lambda)\sigma \end{cases} \tag{2}$$

where r is the distance between two segments, σ is the segment diameter and ϵ is the interaction strength between two segments with a square-well potential interaction; negative ϵ signifies an attraction. The well width parameter, λ, is set to 0.75, a reasonable approximation since there are no long-range segment-segment interactions in non-ionic surfactant / scCO$_2$ systems, the subject of this study.

We choose a hard-sphere potential for the solvent-solvent interaction ($\epsilon_{\rm SS}$) because the simulations are much faster without attractions between solvent molecules than with attractions. Most of the collisions are between solvent molecules due to the low surfactant mole fraction and it is easier computationally to calculate the collision dynamics for a hard-sphere potential than for a square-well potential. In addition the interactions between CO$_2$ molecules are relatively weak (quadrupolar) compared to other interactions in the system, so the neglect of solvent-solvent attractions compared to other interactions is not unreasonable. As we will see, using a hard-sphere potential for the solvent-solvent interaction still permits us to capture the

essential feature of scCO$_2$ density's effect on the phase behavior of polymer / solvent systems. The head-tail interaction is also modeled with a hard-sphere potential since the miscibility of real polymers comprised of the surfactant head or tail beads is generally low.

The variables in our simulations are defined as the following. The homopolymer P$_n$ mole fraction is defined to be $X_{\mathrm{P}_n} \equiv N_{\mathrm{P}_n}/(N_{\mathrm{P}_n} + N_{\mathrm{CO}_2})$ and the surfactant H$_n$T$_m$ mole fraction is defined to be $X_{\mathrm{H}_n\mathrm{T}_m} \equiv N_{\mathrm{H}_n\mathrm{T}_m}/(N_{\mathrm{H}_n\mathrm{T}_m} + N_{\mathrm{CO}_2})$, where N_i is the number of molecules of species i. The homopolymer P$_n$ volume fraction if defined to be $\phi_{\mathrm{P}_n} \equiv nN_{\mathrm{P}_n}/(nN_{\mathrm{P}_n} + N_{\mathrm{CO}_2})$ and the surfactant H$_n$T$_m$ volume fraction is defined to be $\phi_{\mathrm{H}_n\mathrm{T}_m} \equiv (n+m)N_{\mathrm{H}_n\mathrm{T}_m}/[(n+m)N_{\mathrm{H}_n\mathrm{T}_m} + N_{\mathrm{CO}_2}]$. The packing fraction is defined to be $\eta \equiv \pi N_{\mathrm{b}}\sigma^3/6V$, where V is the box volume and N_{b} is the number of beads in the system, $N_{\mathrm{b}} = nN_{\mathrm{P}_n} + N_{\mathrm{CO}_2}$ for homopolymer (P$_n$) / solvent systems and $N_{\mathrm{b}} = (n+m)N_{\mathrm{H}_n\mathrm{T}_m} + N_{\mathrm{CO}_2}$ for surfactant (H$_n$T$_m$) / solvent systems. We limit our study to packing fractions η between 0.2 and 0.5 so as to keep the solvent packing fraction greater than the critical packing fraction ($\eta \approx 0.20$) of a square-well fluid of well width $\lambda = 1.75$ [34] and less than the packing fraction at which a square-well fluid would undergo a transiton to a solid phase. Since the number of surfactant molecules is low compared to the number of CO$_2$ molecules, the (total) packing fraction is a reasonable measure of CO$_2$ density. The reduced temperature is defined to be $T^* \equiv \mathrm{k_B}T/|\epsilon_{\mathrm{HH}}|$, where k$_B$ is Boltzman's constant, T is the temperature, and $|\epsilon_{\mathrm{HH}}|$ is the head-head attraction strength.

In a discontinuous molecular dynamics (DMD) simulation, particles collide when they arrive at a discontinuity in the potential, i.e. the hard-sphere diameter or the square-well width. Between collisions, particles move with linear trajectories, making DMD simulations much faster than traditional molecular dynamics simulations with continuous potentials which re-

quire a small integration time step. The post-collision velocities of particles in DMD are found by solving the collision dynamics equations analytically. To simulate chains of spheres effectively, Rapaport introduced bonds between spheres by limiting the distance between adjacent beads to be between σ and $\sigma(1+\delta)$, where δ is the bond extension parameter.[35] Later Bellemans modified this model so that the distance between adjacent spheres can lie between $\sigma(1-\delta/2)$ and $\sigma(1+\delta/2)$ which makes the average bond length equal to σ.[36]

Since we are interested in simulating at constant temperature system, we use discontinuous canonical molecular dynamics (DCMD),[37–40] an adaptation of the standard DMD technique for the canonical ensemble. The DCMD technique is based on Anderson's stochastic collision method[38] and involves stochastic interaction of the system particles with imaginary constant-temperature heat bath particles. We assume that the system is immersed in an imaginary constant-temperature heat bath containing imaginary "ghost" particles. The ghost particles stabilize the system temperature by colliding with the system particles, resulting in the reassignment of particle velocities according to a Maxwell-Boltzmann distribution about the required temperature. Details of the DCMD method have been described by Gulati et al.[37] and Zhou et al.[40]

Our DMD code was originally developed by Smith and coworkers[41] to treat entangled polymer melts. More recently, it was extended by Schultz et al.[42] to the treatment of copolymers and any mixture of monomers, polymers, and copolymers and optimized to allow for the efficient simulation of large multicomponent systems.

The reduced pressure, P^*, in our simulations is calculated using the virial theorem:

$$P^* \equiv \frac{P\sigma^3}{k_{\rm B}T} = \frac{N_{\rm b}\sigma^3}{V} - \frac{\sigma^3 m \sum_{\rm coll} r_{ij}\Delta v_j}{V k_{\rm B} T t} \tag{3}$$

where $k_{\rm B}$ is Boltzman's constant, T is the temperature, $N_{\rm b}$ is the number of beads, V is the volume, m is the mass of each segment, r_{ij} is the distance between colliding particles i and j, $\Delta v_j = -\Delta v_i$ is the velocity change for the particle j, $\sum_{\rm coll}$ refers to a sum over all collisions, and t is the elapsed simulation time.

Several different types of transitions occur in the homopolymer / solvent and surfactant / solvent systems. In homopolymer / solvent systems, there is a two-phase region representing a phase separated system and a one-phase region where the homopolymer chains are distributed evenly either as aggregates or as unimers in the solvent. When the two phase $\rightarrow$ one phase transition occurs, the homopolymer chains generally exist as aggregates which are evenly distributed throughout the solvent. An additional transition, the aggregate $\rightarrow$ unimer transition can occur as a result of a change of conditions that make the homopolymer more soluble; this transition is characterized by the break-up of the aggregate into unimers. The two phase $\rightarrow$ one phase transition is relatively strightforward to measure experimentally but the aggregate $\rightarrow$ unimer transition is rarely measured in experiments although it can be observed in simulations. In the surfactant / solvent systems, there is also a two-phase region representing a phase separated system and one-phase region where the surfactant chains are distributed evenly either as micelles or unimers in the solvent. If the surfactants form micelles when the two phase $\rightarrow$ one phase transition occurs, the one-phase region is a micelle phase. An additional transition can occur, the micelle $\rightarrow$ unimer transition, as a result of a change in conditions that make the

surfactants more soluble in the solvent.

The two phase $\rightarrow$ one phase transition for the surfactant / solvent systems is located by calculating the contrast structure factor. The structure factor is the Fourier transform of the radial distribution function. According to Murat and coworkers[43], the structure factor of a multicomponent system can be evaluated using the following equation:

$$S(\vec{q}) = \frac{1}{N} \sum_{j,k} \langle b_j b_k \rangle \, e^{i\vec{q}\cdot\vec{r}_{jk}} \tag{4}$$

where $\vec{q}$ is the wave vector, b is a labelling variable for each component in the system, and $\vec{r}_{jk}$ is the vector between particles j and k. This formula involves taking a double sum over all j and k particles. For a system with many particles, this calculation can become costly. Instead, we follow McGreevy[44] and use the following equivalent formula:

$$S(\vec{q}) = \frac{1}{N} \left| \sum_{j} b_j e^{i\vec{q}\cdot\vec{r}_j} \right|^2 \tag{5}$$

The value of b_j for the different components can be chosen to be 1, -1 and 0. If b_j equals zero for particle j of component A, then component A is ignored in the structure factor calculation. If b_j is non-zero for one only component, we obtain the structure factor for that component only. A contrast structure factor (showing the difference between the distribution of two components A and B) can be obtained by setting $b_j = 1$ if particle j is component A and $b_j = -1$ if particle j is component B. If a total density structure factor is desired (which is only sensitive to variations in the total density), then one can set $b_j = 1$ for particles of component A or B and $b_j = 0$ for particles that are solvent (or vacancies in a lattice simulation). In our work we focus

on the contrast structure factor ($S_{\mathrm{H+T-S}}$) which highlights the contrast between the distribution of head (H) and tail (T) beads in surfactant chains and the distribution of solvent molecules (S) in the system. This can be obtained by setting $b_j = 1$ for surfactant head and tail beads and $b_j = -1$ for solvent beads in Equation 5.

To calculate the structure factor, DMD simulations were performed on the surfactant / solvent system of interest at the desired conditions (surfactant mole fraction, packing fraction and reduced temperature) until equilibrium was reached. A snapshot of the configuration of the equilibrated system was obtained, which displays the surfactant distribution in the solvent. The contrast structure factor was then calculated by applying Equation 5 with $b_j = 1$ for surfactant head and tail beads and $b_j = -1$ for solvent beads.

To illustrate how the structure factor calculation is used to located the two phase $\rightarrow$ one phase transition, consider the snapshots shown in figure 1 for a surfactant ($\mathrm{H_4T_8}$) / solvent system at (a) η = 0.24 and (b) η = 0.27. At $\eta = 0.24$, almost all the surfactant molecules aggregate tightly in the system which is indicative of phase separation. At η = 0.27, the surfactant molecules form micelles, which are distributed evenly throughout the system, with the head block as the core and the tail block as the corona. The snapshots at η = 0.24 and 0.27, tell us that the system at η = 0.24 is in a two-phase region and that the system at η = 0.27 is in the micelle region. In the snapshots for the systems at η = 0.25 and 0.26 (not shown), the aggregates formed by the surfactants in the system are loose compared with that for η = 0.24 and the tail corona of different aggregates are connected, making it difficult to determine whether this is the two-phase region or the micelle phase. The contrast structure factors for the $\mathrm{H_4T_8}$ / solvent system at (a) η = 0.26 and (b) η = 0.27 are shown in figure 2. In the contrast structure factor

diagram, which plots the contrast structure factor versus the reduced frequency, the lowest frequency corresponds to the box length, which is the maximum possible wave length. A sharp peak occuring at the lowest frequency indicates that the system is phase separated. We see that the contrast structure factor at η = 0.25 has a sharp peak at the lowest frequency ($q\sigma$ = 0.2) but that no peak occurs at the lowest frequency ($q\sigma$ = 0.2) at η = 0.26. Based on the snapshots and contrast structure factors in Figure 1 and 2, the packing fraction at which the transition from the two-phase to the one-phase region, $\eta_{2\phi\rightarrow1\phi}$, is located between 0.25 and 0.26.

Typical steps for the location of the transition from the two-phase region to the one-phase region are the following. First we perform simulations at η = 0.25, 0.35 and 0.45 examining configurational snapshots at each condition to narrow in on the two-phase region and/or the micelle region. If, for example, we find a two-phase region at $\eta = 0.25$ and a micelle region at $\eta = 0.35$, then simulations would be performed at η = 0.28 and 0.31 and snapshots examined at these conditions. Once we get to a set of conditions, e.g. η = 0.29 and 0.30 where we can not differentiate between the two phase and micelle region, contrast structure factors would be examined to pinpoint the packing fraction at which the two-phase to the one-phase region takes place.

To locate the micelle $\rightarrow$ unimer transition, we calculate the aggregate size distribution at different η (chosen to be higher than $\eta_{2\phi\rightarrow1\phi}$). The aggregate size distribution is represented by a plot of the volume fraction of micelles containing M surfactant molecules, ϕ_{M}, versus M where the micelle volume fraction is defined to be the volume occupied by micelles containing M surfactant molecules divided by the total volume occupied by the micelles in the system. To calculate the number of surfactants in a micelle, we calculate the distance between any head

bead of chain A and any head bead of chain B, $d_{\mathrm{H_A H_B}}$. If $d_{\mathrm{H_A H_B}}$ is greater than the square-well width, $(1+\lambda)\sigma$, the chain A and B are considered to be in the same micelle say M_i. Similiar calculations are performed for all pairs of chains in the system. For the homopolymer / solvent system, we calculate the distance between any bead on homopolymer chain A and B instead of any head bead on surfactant chain A and B.

To illustrate how the micelle $\rightarrow$ unimer transition is calculated, consider the aggregate size distributions shown in figure 3 for a surfactant $\mathrm{H_4T_8}$ / solvent system in the $\phi_{\mathrm{M}} - M$ plane at packing fractions, η = 0.29, 0.30 and 0.31. For η = 0.31, the aggregate size distribution exhibits only one peak at very small M, which represents unimers. At η = 0.30, the peak at very small M is lowered and a small bump occurs at a higher value of M, indicating that small aggregates begin to form in the system. For η = 0.29, the first peak is lower still and a second (micellar) peak occurs, indicating that spherical micelles are formed in the system. In this study, we choose the location of the micelle $\rightarrow$ unimer transition to be the packing fraction at which the second peak just dissapears in the aggregate size distribution. In figure 3 the packing fraction at which the micelle $\rightarrow$ unimer transition occurs is 0.30 for this $\mathrm{H_4T_8}$ / solvent system.

For the homopolymer / solvent systems, the two phase $\rightarrow$ one phase transition can be located by comparing the configurational snapshots at different conditions. The difference between the snapshots for the conditions in the two-phase region and one-phase region at which conditions close to the two phase $\rightarrow$ one phase transition is easy to distinguish. The steps in locating for the two phase $\rightarrow$ one phase transition for homopolymer / solvent systems are similiar to that of surfactant / solvent systems except there is no need to calculate the contrast structure factor at the end. To locate the aggregate $\rightarrow$ unimer transition, we calculate the

aggregate size distribution at different η (chosen to be higher than $\eta_{2\phi\rightarrow 1\phi}$) in a manner similiar to the calculation of the micelle size distribution.

Discontinuous molecular dynamics simulations were performed in the canonical ensemble (constant N, V, T) on systems containing homopolymer P_n plus solvent where $n = 4$ and 8 and on systems containing surfactant chains H_4T_8, H_3T_9 and H_3T_6 plus solvent molecules, all at packing fractions, η, in the range of $0.2-0.5$. The simulations were started in a random configuration containing 500 solvent molecules and 6, 9 or 12 chains at the desired packing fraction and reduced temperature. Once the system was equilibrated, as indicated by a lack of fluctuation in the aggregate or micelle size distribution, the unit subcell was replicated two (or three) times in every direction yielding 4000 solvent molecules and 48, 72 or 96 chains (or 13500 solvent molecules and 162, 243 or 324 chains). The simulation on the bigger system was then continued until equilibrium was reached, as indicated by a lack of fluctuation in the aggregate or micelle size distribution. At the end of this process, a snapshot displaying the distribution of chains in the solvent was taken, and the contrast structure factor or aggregate or micelle size distribution was calculated to determine which phase the system was in. The two phase $\rightarrow$ one phase transition and the micelle $\rightarrow$ unimer transition for surfactant / solvent systems and the two phase $\rightarrow$ one phase transition and the aggregate $\rightarrow$ unimer transition for for homopolymer / solvent systems were recorded as a function of homopolymer or surfactant mole fraction, packing faction and reduced temperature. The average CPU time needed on our 600 MHz Alpha 21164 included 1 h for the equilibration of the small systems, 10h for the equilibration of the large system which is 8 times the size of the small system, and 30h for the large system which is 27 times the size of the small system at each state point.

The phase diagrams described in the next section were created by performing the simulations described above over a wide variety of temperatures and packing fractions. The desired range for packing fraction is $0.2-0.5$. Most simulations were performed at a reduced temperature of 1.0 except for the simulations performed to investigate the effect of temperature variation on the phase behavior.

3 Results and Discussion

3.1 Homopolymer

In order to establish appropriate polymer-polymer and polymer-solvent interaction parameters and to ensure that $\eta_{2\phi\rightarrow 1\phi}$ and $\eta_{\mathrm{m}\rightarrow\mathrm{u}}$ are in the desired range of $0.2-0.5$, we first simulated homopolymer / $scCO_2$ systems. The two phase $\rightarrow$ one phase transition for a homopolymer / solvent system was located by monitoring the configurational snapshots at different η as described in Section 2.

Figure 4 shows the transitions for homopolymers of length 4, P_4, from the two-phase region to the one-phase region in the $X_{\mathrm{P}_4}-\eta$ plane at three different parameter sets $(\epsilon_{\mathrm{PP}}, \epsilon_{\mathrm{PS}}) = (-0.9,-0.6),(-1.0,-0.6)$ and $(-1.0,-0.55)$. This shows that the number of homopolymer molecules that can dissolve in the solvent increases at higher η, and that X_{P_4} increases as $\eta_{2\phi\rightarrow 1\phi}$ increases. This trend is in agreement with experimental observations on PVAc, whose solubility increases as $scCO_2$ density increases[14]. The polymer dissolves in the solvent as η increase at fixed homopolymer mole fraction, because this increases the solvent density around

each homopolymer molecule, establishing more attractions between the polymer molecule and solvent and screening the more attractive polymer-polymer interaction.

Figure 4 shows that the homopolymers with stronger polymer-polymer attraction or weaker polymer-solvent attraction need higher packing fractions to dissolve. This is because homopolymer molecules with strong $|\epsilon_{\rm PP}|$ or weak $|\epsilon_{\rm PS}|$ are more likely to attract other polymer molecules than to attract solvent molecules, and hence to form aggregates which have lower solvent affinity.

Figure 5 shows the transitions from the two-phase region to the one-phase region in the $\phi_{\rm P}$-η plane for homopolymer P_4 with parameter set $(\epsilon_{\rm PP}, \epsilon_{\rm PS}) = (-0.9, -0.6)$ and homopolymer P_8 with two different parameter sets $(\epsilon_{\rm PP}, \epsilon_{\rm PS}) = (-0.9, -0.6)$ and $(-1.0, 0.6)$. We choose the volume fraction instead of the mole fraction here since we want to compare the solubilities of homopolymers with different chain lengths based on the same homopolymer concentration in the solvent. We find again that more homopolymer molecules can dissolve in $scCO_2$ at higher η, and that a homopolymer with a stronger $|\epsilon_{\rm PP}|$ requires a higher value of η to dissolve for both P_4 as seen in figure 4 and P_8. We also find that the packing fraction at which the transition from the two-phase region to the one-phase region occurs, $\eta_{2\phi\rightarrow 1\phi}$, for long chains ($P_8$) is higher than for short chains (P_4) at any given value of $\phi_{\rm P}$, in qualitative agreement with experimental results[14] that the PVAc solubility decreases as its chain length increases.

Figure 6 displays the aggregate $\rightarrow$ unimer transition for homopolymer P_4 in the space spanned by the polymer-polymer attraction strength ($|\epsilon_{\rm PP}|$) and the polymer-solvent attraction strength ($|\epsilon_{\rm PS}|$) at $X_{\rm P_4}$= 0.089, η = 0.214, 0.314 and 0.414, and T^* = 1.0. The homopolymers assemble into aggregates as $|\epsilon_{\rm PP}|$ increases or as $|\epsilon_{\rm PS}|$ decreases as described previously. We

also find that the unimer region extends to higher values of $|\epsilon_{\rm PP}|$ and lower values of $|\epsilon_{\rm PS}|$ as the packing fraction increases since homopolymer solubility increases as the packing fraction increases.

Figure 7 displays the aggregate $\rightarrow$ unimer transition for homopolymers P_4 and P_8 in the $|\epsilon_{\rm PP}| - |\epsilon_{\rm PS}|$ plane at homopolymer volume fraction $\phi_{\rm P}$ = 0.0347, η = 0.414, and T^* = 1.0. The aggregate $\rightarrow$ unimer transition shifts to weaker polymer-polymer attraction and stronger polymer-solvent attraction as the homopolymer chain length is increased since longer chains have lower solubility than short chains.

Figure 8 displays the transition from the two-phase region to the one-phase region in the $X_{\rm P_4} - \eta$ plane for homopolymers $\rm P_4$ with the parameter set $(\epsilon_{\rm PP}, \epsilon_{\rm PS}) = (-1.0, -0.5)$ at different simulation temperatures T^* = 1.1, 1.2 and 1.4. We find that more homopolymer molecules are dissolved in the solvent at higher T^* at fixed packing fraction and that $\eta_{2\phi\rightarrow 1\phi}$ decreases as T^* increases. This means that in our model the homopolymer solubility increases as temperature increases at fixed packing fraction, in agreement with experimental results on the solubility of 1,4-bis-(octylamino)-9,10-anthraquinone (AQ08) in $\rm scCO_2$.[45]

Figure 9 displays the transition from the two-phase region to the one-phase region for homopolymer $\rm P_4$ in: (a) the $\eta - T^*$ plane, and (b) the $P^* - T^*$ plane for $(\epsilon_{\rm PP}, \epsilon_{\rm PS}) = (-1.0, -1.0)$ and $(-1.0, -0.5)$ at fixed homopolymer mole fraction $X_{\rm P_4} = 0.01768$. Figure 9a shows that $\eta_{2\phi\rightarrow 1\phi}$ decreases as T^* increases for both parameter sets. Figure 9b shows that the phase transition lines in a $P^* - T^*$ diagram have a negative slope, indicating that the homopolymers discussed in figure 9 show upper-critical-solution-temperature (UCST) behavior.

3.2 Surfactant

The head block and tail block parameters for our surfactant simulations are chosen in the following way. The head block parameters are chosen to be those of a homopolymer that dissolves in solvent only at high η; the tail block parameters are chosen to be those of a homopolymer that dissolves in solvent at low η. Based on our simulation results for the homopolymer / solvent systems described in Section 3.1, our H_4T_8 surfactant molecules are modeled by covalently connecting a homopolymer P_4 with $(\epsilon_{\rm PP}, \epsilon_{\rm PS}) = (-1.0, -0.5)$ as the slightly CO_2-philic head block and a homopolymer P_8 with $(\epsilon_{\rm PP}, \epsilon_{\rm PS}) = (-0.1, -1.0)$ as the more CO_2-philic tail block.

We determined the location of the transition from the two-phase region to the one-phase region for surfactant H_4T_8 by monitoring the contrast structure factors and the configurational snapshots, and the location of the micelle $\rightarrow$ unimer transition by monitoring the aggregate (micelle) size distribution as described in Section 2. Figure 10 shows that the surfactant / solvent system goes from a two-phase region at low η to a micelle phase at intermediate η and to a unimer phase at even higher η. The three regions (two-phase region, micelle phase and unimer phase) are divided by the $2\phi \rightarrow 1\phi$ transition line and the micelle $\rightarrow$ unimer transition line. We also find that the packing fraction at which the $2\phi \rightarrow 1\phi$ transition or the micelle $\rightarrow$ unimer transition occurs increases as $X_{\rm H_4T_8}$ increases. This phase diagram is consistent with the experimental phase diagram of PVAc-*b*-PTAN in $scCO_2$[14]. The trend that the packing fraction at which the micelle $\rightarrow$ unimer transition occurs increases as $X_{\rm H_4T_8}$ increases in our simulations is in qualitative agreement with the trend that the CMC increases as $scCO_2$ density

increases in experiments[14].

It is of interest to be able to relate the phase behavior of a surfactant / solvent system to the phase behavior (i.e., the solubilities) of the homopolymers that make up the surfactant head or tail block. Figure 11 shows the $2\phi \rightarrow 1\phi$ transition and the micelle $\rightarrow$ unimer transition for H_4T_8 on the same diagram as the $2\phi \rightarrow 1\phi$ transition of the more CO_2-philic P_8 and the aggregate $\rightarrow$ unimer transition of the slightly CO_2-philic P_4. We choose the aggregate $\rightarrow$ unimer transition of P_4 rather than its $2\phi \rightarrow 1\phi$ transition to compare with the micelle $\rightarrow$ unimer transition of H_4T_8 since the homopolymers in the one-phase region close to the $2\phi \rightarrow 1\phi$ transition are mostly aggregates in the solvent rather than unimers. The four transitions occur in the following order as η increases: (1) the $2\phi \rightarrow 1\phi$ transition of P_8, (2) the $2\phi \rightarrow 1\phi$(micelle) transition of H_4T_8, (3) the micelle $\rightarrow$ unimer transition of H_4T_8 and (4) the aggregate$\rightarrow$unimer transition of P_4. The $\eta_{2\phi\rightarrow 1\phi}$ for H_4T_8 is higher than that for P_8 since adding the slightly CO_2-philic P_4 to the more CO_2-philic P_8 makes the H_4T_8 solubility lower in scCO_2 than P_8. The $\eta_{\mathrm{m}\rightarrow\mathrm{u}}$ for H_4T_8 is lower than the $\eta_{\mathrm{a}\rightarrow\mathrm{u}}$ for P_4 since adding the more CO_2-philic P_8 to the slightly CO_2-philic P_4 makes the solvent affinity of H_4T_8 higher than P_4. The surfactant dissolves as a unimer in the solvent easier than P_4 dissolves in the solvent as a unimer. It is apparent that the phase behavior of a surfactant / solvent system is directly related to the solubilities of the corresponding homopolymers that serve as head and tail block for the surfactant.

To study how the strength of the head-solvent attraction, $|\epsilon_{\mathrm{HS}}|$, affects the phase behavior of the H_4T_8 / solvent system, we performed simulations at different values of ϵ_{HS} at fixed ϵ_{HH}, ϵ_{TT} and ϵ_{TS} . Figure 12 shows the phase behaviors for the three surfactants with: (a) $\epsilon_{\mathrm{HS}} = -0.4$, (b) $\epsilon_{\mathrm{HS}} = -0.5$, and (c) $\epsilon_{\mathrm{HS}} = -0.6$ holding the other three parameters fixed at

$\epsilon_{\mathrm{HH}} = -1.0$, $\epsilon_{\mathrm{TT}} = -0.1$ and $\epsilon_{\mathrm{TS}} = -1.0$. For $\epsilon_{\mathrm{HS}} = -0.4$, there is a two-phase region and a micelle region as η increases; no unimer phase is found over the entire η range $(0.2 - 0.5)$. For $\epsilon_{\mathrm{HS}} = -0.5$, there is a two-phase region, a micelle phase and a unimer phase as η increases. For $\epsilon_{\mathrm{HS}} = -0.6$, there is a two-phase region and a unimer region as η increases; no micelle phase is found. Figure 12 shows that the value of $|\epsilon_{\mathrm{HS}}|$ strongly affects the phase behavior of surfactants in scCO$_2$. If the head-solvent attraction is weak, the surfactants cannot be dissolved as unimers even at relatively high η, which means that the micelle $\rightarrow$ unimer transition moves to high η values beyond the range of interest. If the head-solvent attraction is very strong, the surfactants dissolve in scCO$_2$ as unimers without forming micelles as η increases and the micelle $\rightarrow$ unimer transition disappears.

To study how the strengths of the tail-tail attraction, $|\epsilon_{\mathrm{TT}}|$, and the tail-solvent attraction, $|\epsilon_{\mathrm{TS}}|$, affect the location of the micelle $\rightarrow$ unimer transition, we performed simulations at two different values for $\epsilon_{\mathrm{TT}} = -0.1$ and -0.2, at fixed $\epsilon_{\mathrm{TS}} = -1.0$, and at two different values for $\epsilon_{\mathrm{TS}} = -0.8$ and -1.0, at fixed $\epsilon_{\mathrm{TT}} = -0.1$. Figure 13 shows the micelle $\rightarrow$ unimer transition in the $X_{\mathrm{H_4T_8}} - \eta$ plane for different surfactants with different interaction parameter sets: (a) (ϵ_{TT}, ϵ_{TS}) $= (-0.1, -1.0)$, and $(-0.2, -1.0)$ and (b) (ϵ_{TT}, ϵ_{TS}) $= (-0.1, -1.0)$ and $(-0.1, -0.8)$. The packing fraction at which the micelle $\rightarrow$ unimer transition occurs is slightly lowered by decreasing $|\epsilon_{\mathrm{TT}}|$ or increasing $|\epsilon_{\mathrm{TS}}|$. The tail block's affinity for the solvent increases as $|\epsilon_{\mathrm{TS}}|$ increases or as $|\epsilon_{\mathrm{TT}}|$ decreases and this helps to dissolve the entire surfactant molecule in the solvent. Unlike the value of $|\epsilon_{\mathrm{HS}}|$, which strongly affects the location of the micelle $\rightarrow$ unimer transition, $|\epsilon_{\mathrm{TT}}|$ and $|\epsilon_{\mathrm{TS}}|$ only affect the location of the micelle $\rightarrow$ unimer transition weakly.

The importance of the various parameters in determining the location of the micelle $\rightarrow$

unimer transition can be ranked based on the simulations performed on the surfactant with different parameter sets. As the phase behavior of the surfactant / solvent system in figure 12 and 13 shows, the location of the micelle $\rightarrow$ unimer transition is either beyond the η range of interest for weak head-tail attraction or disappears for strong head-solvent attraction, while it is only weakly affected by the strengths of the tail-tail and tail-solvent attractions. This tells us that the micelle $\rightarrow$ unimer transition of a surfactant / solvent system depends more upon the solvent affinity of its head block than on the solvent affinity of its tail block.

To explore the influence of surfactant architecture as measured by the head length / tail length ratio (f) and total chain length ($n+m$) on the micelle $\rightarrow$ unimer transition of a surfactant / $scCO_2$ system, we performed simulations on three different surfactants H_4T_8, H_3T_9 and H_3T_6. Figure 14 shows a comparison between the location of the micelle $\rightarrow$ unimer transition in the $X_{\mathrm{H_nT_m}} - \eta$ plane for different surfactant architectures: (a) H_4T_8 and H_3T_9 ($f = 1/2$ and $1/3$, $n + m = 12$) and (b) H_3T_6 and H_4T_8 ($f = 1/2$, $n + m = 9$ and 12). The packing fraction at which the micelle $\rightarrow$ unimer transition occurs for H_4T_8 is higher than that for H_3T_9 and that for H_3T_6. The packing fraction at which the micelle $\rightarrow$ unimer transition occurs increases as f increases at fixed $n + m$ or as $n + m$ increases at fixed f, which is in agreement with experimental results that the solubility of Ls-36 higher than that of Ls-45 in $scCO_2$, where $C_{12}H_{25}$-O-$(EO)_n(PO)_m$H, EO is ethylene oxide group and PO is propylene oxide group, $n = 3, m = 6$ for Ls-36 and $n = 4, m = 5$ for Ls-45.[46] Increasing f at fixed $n+m$ for a surfactant decreases the solvent affinity of the surfactants since the slightly solvent-philic block is longer while the solvent-philic block is shorter. By increasing $n+m$ at fixed f, we obtain a surfactant with longer head and tail blocks. Since the solubility of long-chain homopolymers in solvent is

lower than that of short-chain homopolymers, as discussed in Section 3.1, the solvent affinities of both the head block and the tail block of a long-chain surfactant are decreased thus the entire surfactant molecule has lower solvent affinity than a short-chain surfactant with the same f.

Figure 15 shows the location of the transition from the two-phase region to the one-phase (micelles) region in the $X_{\mathrm{H_4T_8}} - \eta$ plane for the H_4T_8 / solvent system at two different simulation temperatures, T^* = 0.9 and 1.1. The packing fraction at which the transition from the two-phase region to the one-phase (micelles) region occurs decreases as T^* increases and the surfactant solubility in $scCO_2$ increases as T^* increases at fixed η. This result is in agreement with experiment results on Ls-36 and Ls-45 surfactants in $scCO_2$ which show that the surfactant solubility increases as temperature increases at fixed fluid denstiy[46].

Figure 16 shows the locations of both the $2\phi \rightarrow 1\phi$(micelle) transition and the micelle $\rightarrow$ unimer transition in the $\eta - T^*$ plane for the H_4T_8 / solvent system. There are three different regions: the two-phase region at low η and low T^*, the micelle phase at intermediate η and intermediate T^*, and the unimer phase at high η and high T^*. Since homopolymer solubility increases with increasing η, as discussed in Section 3.1, the solvent density around a surfactant molecule increases as η increases, resulting in an increase in the solvent affinities of the surfactant head and tail block as η increases. This results in the two-phase region, micelle phase and unimer phase occuring as η increases at fixed temperature. As indicated in Section 3.1, the solubility of the head and tail blocks increase as temperature increases at constant η resulting a two-phase region, micelle phase and unimer phase as T^* increases at constant η.

Figure 17 shows the phase behavior of the H_4T_8 / solvent system in the $X_{\mathrm{H_4T_8}} - T^*$ plane at η = 0.30. The surfactant / solvent system goes from a two-phase region at low T^* to a

micelle phase at intermediate T^* and then to a unimer phase at even higher T^* since the solubilities of the head and tail block increase as T^* increases. We find both the micelle $\rightarrow$ unimer transition and the transition from a two-phase region to a one-phase region, consisent with experiments.[28] This is in contrast to the simulation results on the incompressible model surfactant / solvent system by Panagiotopoulos et al[27], who found either micellization or phase separation in their simulations on model surfactant / systems at a fixed set of interaction parameters, but never both. We also find that the surfactant mole fraction at which the micelle $\rightarrow$ unimer transition occurs increases as T^* increase. This trend agrees with the trend observed by Panagiotopoulos et al[27] that the surfactant volume fraction at the CMC increases with increasing temperature.

The discrepancy between our simulation results and the simulations of Panagiotopoulos et al.[27] is due to the difference in the models employed in the simulations. In our model the head-head (solvent-phobic block), head-solvent, tail-tail (solvent-philic block) and tail-solvent attractions are included; whereas in their model the only attraction considered is between the solvent-phobic tail block segments. In our model, temperature can affect the solvent affinities of both the head and tail blocks while in their model temperature can only affect the solvent affinity of the tail block. Panagiotopoulos et al.[27] hypothesized that the disagreement between their simulation results and the experimental observations of both the $1\phi \rightarrow 2\phi$ and unimer $\rightarrow$ micelle transition was due to their neglect of the unusual solvation properties of water, in particular that water's solvation power decreases with increasing temperature. Instead, based on our results, it appears that the most likely explanation is their neglect of the interactions related to the solvent-philic block.

4 Summary

We have performed DMD simulations on model surfactant / solvent systems with varying interaction strengths and surfactant structure (head length / tail length ratio and overall chain length) at different surfactant mole fractions, packing fractions and reduced temperatures. The phase diagrams constructed for the surfactant / solvent systems in the surfactant mole fraction−packing fraction plane are consistent with the experimentally observed phase diagram for the PVAc-PTAN / scCO_2 system in the surfactant concentration−CO_2 density plane[14]. We show that the phase behavior for a surfactant / solvent system is directly related to the solubilities of the corresponding homopolymers that serve as the head and tail block for the surfactant.

The phase behavior for the surfactants with different interaction parameter sets shows that the location of the micelle → unimer transition is beyond the packing fraction range of interest for weak head-solvent attraction and disappears for strong head-solvent attraction, but is only weakly affected by the strengths of the tail-tail and tail-solvent attractions. This tells us that the micelle → unimer transition of a surfactant / solvent system depends more upon the solvent affinity of its head block than on the solvent affinity of its tail block. The packing fraction at which the micelle → unimer transition occurs increases as the surfactant head/tail ratio increases at fixed surfactant chain length or as the surfactant chain length increases at fixed surfactant head/tail ratio, in qualitative agreement with experiment observations on effect of head/tail ratio on the surfactant solubility in scCO_2.[46] The solubilities of homopolymers and surfactants increase as packing fraction increases at fixed temperature and as temperature

increases at fixed packing fraction, in agreement with experiments on the effect of temperature on non-inonic surfactant solubilities in $scCO_2$.[47]

Both micellization and phase separation are found in our simulations upon decreasing temperature in contrast to the simulations of Panagiotopoulos et al.[27] This indicates that including interactions for both blocks of a surfactant is important to the description of the phase behavior of a surfactant / solvent system.

References

[1] Eckert, C. A. , Knutson, B. L. , and Debenedetti, P. G. , *Nature*, **383**, 313 (1996).

[2] McHugh, M. K. and Krukonis, V. J. , In *Supercritical Fluid Extraction: Principles and Practice.* Butterworths, Stoneham, MA, (1994).

[3] Hoefling, T. , Stofesky, D. , Reid, M. , Beckman, E. , and Enick, R. M. , *J. Supercrit. Fluids*, **5**, 237 (1992).

[4] Desimone, J. M. , Guan, Z. , and Elsbernd, C. S. , *Science*, **257**, 945 (1992).

[5] Hoefling, T. A. , Newman, D. A. , Enick, R. M. , and Beckman, E. J. , *J. Supercrit. Fluids*, **6**, 165 (1993).

[6] Hsiao, Y. L. , Maury, E. E. , DeSimone, J. M. , Mawson, S. , and Johnston, K. P. , *Macromolecules*, **28**, 8159 (1995).

[7] Xiong, Y. and Kiran, E. , *Polymer*, **36**, 4817 (1995).

[8] ChilluraMartino, D. , Triolo, R. , McClain, J. B. , Combes, J. R. , Betts, D. E. , Canelas, D. A. , DeSimone, J. M. , Samulski, E. T. , Cochran, H. D. , and Londono, J. D. , *J. Mol. Struct.*, **383**, 3 (1996).

[9] Dardin, A. , Cain, J. B. , DeSimone, J. M. , and Johnson, C. S. , *Macromolecules*, **30**, 3593 (1997).

[10] McClain, J. B. , Betts, D. E. , Canelas, D. A. , DeSimone, E. T. S. J. M. , Londono, J. D. , Cochran, H. D. , Wignall, G. D. , ChilluraMartino, D. , and Triolo, R. , *Science*, **274**, 2049 (1996).

[11] Triolo, F. , Triolo, A. , Triolo, R. , Londono, J. D. , Wignall, G. D. , McClain, J. B. , Betts, D. E. , Wells, S. , Samulski, E. T. , and DeSimone, J. M. , *Langmuir*, **16**, 416 (2000).

[12] Triolo, R. , Triolo, A. , Triolo, F. , Steytler, D. C. , Lewis, C. A. , Heenan, R. K. , Wignall, G. D. , and DeSimone, J. M. , *Phys. Rev. E*, **61**, 4640 (2000).

[13] Triolo, A. , Triolo, F. , Celso, F. L. , Betts, D. E. , McClain, J. B. , DeSimone, J. M. , Wignall, G. D. , and Triolo, R. , *Phys. Rev. E*, **62**, 5839 (2000).

[14] Buhler, E. , Dobrynin, A. V. , DeSimone, J. M. , and Rubinstein, M. , *Macromolecules*, **31**, 7347 (1998).

[15] Colina, C. M. , Hall, C. K. , and Gubbins, K. E. , *Fluid Phase Equilib.*, **194**, 553 (2002).

[16] Salaniwal, S. , Cui, S. T. , Cochran, H. D. , and Cummings, P. T. , *Langmuir*, **17**, 1773 (2001).

[17] Salaniwal, S. , Cui, S. T. , Cochran, H. D. , and Cummings, P. T. , *Langmuir*, **17**, 1784 (2001).

[18] Lisal, M. , Hall, C. K. , Gubbins, K. E. , and Panagiotopoulos, A. Z. , *J. Chem. Phys.*, **116**, 1171 (2002).

[19] Lisal, M. , Hall, C. K. , Gubbins, K. E. , and Panagiotopoulos, A. Z. , *Fluid Phase Equilib.*, **194**, 233 (2002).

[20] LARSON, R. G. , SCRIVEN, L. E. , and DAVIS, H. T. , *J. Chem. Phys.*, **83**, 2411 (1985).

[21] Larson, R. G. , *Curr. Opin. Colloid. In.*, **2**, 361 (1997).

[22] Bhattacharya, A. , Mahanti, S. D. , and Chakrabarti, A. , *J. Chem. Phys.*, **108**, 10281 (1998).

[23] Bhattacharya, A. and Mahanti, S. D. , *J. Phys.: Condens. Matter*, **13**, 861 (2001).

[24] Rajagopalan, R. , Rodriguez-Guadarrama, L. A. , and Talsania, S. K. , *Handbook of microemulsion science and technology*. Marcel Dekker, New York, (1999).

[25] Talsania, S. K. , Rodriguez-Guadarrama, L. A. , Mohanty, K. K. , and Rajagopalan, R. , *Langmuir*, **14**, 2648 (1998).

[26] Floriano, M. A. , Caponetti, E. , and Panagiotopoulos, A. Z. , *Langmuir*, **15**, 3143 (1999).

[27] Panagiotopoulos, A. Z. , MA, M. A. F. , and Kumar, S. K. , *Langmuir*, **18**, 2940 (2002).

[28] Israelachvili, J. , *Intermolecular and surface forces, 2nd ed.* Wiley, New York, (1989).

[29] Salaniwal, S. , Cui, S. T. , Cochran, H. D. , and Cummings, P. T. , *Ind. Eng. Chem. Res.*, **39**, 4543 (2000).

[30] Senapati, S. , Keiper, J. S. , DeSimone, J. M. , Wignall, G. D. , Melnichenko, Y. B. , Frielinghaus, H. , and Berkowitz, M. L. , *Langmuir*, **18**, 7371 (2002).

[31] Eastoe, J. , Bayazit, Z. , Martel, S. , Stytler, D. C. , and Heenan, R. K. , *Langmuir*, **12**, 1423 (1996).

[32] Rindfleisch, F. , DiNoia, T. P. , and McHugh, M. A. , *J. Phys. Chem.*, **100**, 15581 (1996).

[33] O'Neill, M. L. , Cao, Q. , Fang, M. , and Johnston, K. P. , *Ind. Eng. Chem. Res.*, **37**, 3067 (1998).

[34] Vega, L. , de Miguel, E. , and Rull, L. F. , *J. Chem. Phys.*, **96**, 2296 (1992).

[35] Rapaport, D. C. , *J. Chem. Phys.*, **71**, 3299 (1979).

[36] Bellemans, A. , Orban, J. , and Belle, D. V. , *Mol. Phys.*, **39**, 781 (1980).

[37] Gulati, H. S. and Hall, C. K. , *J. Chem. Phys.*, **107**, 3930 (1997).

[38] Anderson, H. C. , *J. Chem. Phys.*, **72**, 2384 (1980).

[39] Zhou, Y. Q. , Hall, C. K. , and Karplus, M. , *Phys. Rev. Lett.*, **77**, 2822 (1996).

[40] Zhou, Y. Q. , M, M. K. , Wichert, J. M. , and Hall, C. K. , *J. Chem. Phys.*, **107**, 10691 (1997).

[41] Smith, S. W. , Freeman, B. D. , and Hall, C. K. , *J. Comput. Phys.*, **134**, 16 (1997).

[42] J.Schultz, A. , Hall, C. K. , and Genzer, J. , *J. Chem. Phys.*, **117**, 10329 (2002).

[43] Murat, M. , Grest, G. S. , and Kremer, K. , *Macromolecules*, **32**, 595 (1999).

[44] McGreevy, R. L. , In Catlow, C. R. A. , editor, *Computer Modelling in Inorganic Crystallography.* Academic Press, San Diego, (1997).

[45] Schneider, G. M. , Kautz, C. B. , and Tuma, D. , In E, K. , Debenedetti, P. G. , and CJ, P. , editors, *Supercritical Fluids: Fundamentals and application*, page 49. Kluwer Acadamic, the netherland, (1998).

[46] Liu, J. C. , Han, B. X. , Wang, Z. W. , Zhang, J. L. , Li, G. Z. , and Yang, G. Y. , *Langmuir*, **18**, 3086 (2002).

[47] Liu, J. C. , Han, B. X. , Li, G. Z. , Liu, Z. M. , He, J. , and Yang, G. , *Fluid Phase Equilib.*, **187**, 247 (2001).

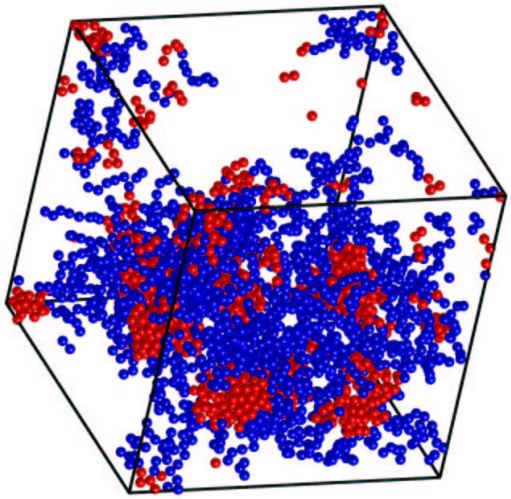

(a) η=0.24

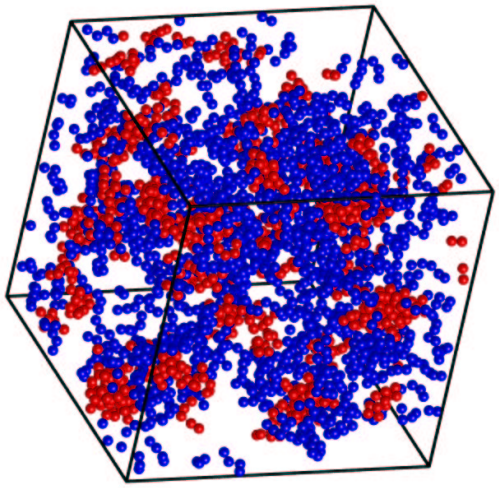

(b) η=0.27

Figure 1: Snapshot of the H_4T_8/solvent system containing 15,444 beads at (a) $\eta = 0.24$ and (b) $\eta = 0.27$ at $X_{\mathrm{H_4T_8}} = 0.0119$ and $T^* = \mathrm{k}T/|\epsilon_{\mathrm{HH}}| = 1.0$ for the parameter set $\epsilon_{\mathrm{HH}} = -1.0, \epsilon_{\mathrm{HS}} = -0.5$, $\epsilon_{\mathrm{TT}} = -0.1$ and $\epsilon_{\mathrm{TS}} = -1.0$. (Solvent molecules are not shown).

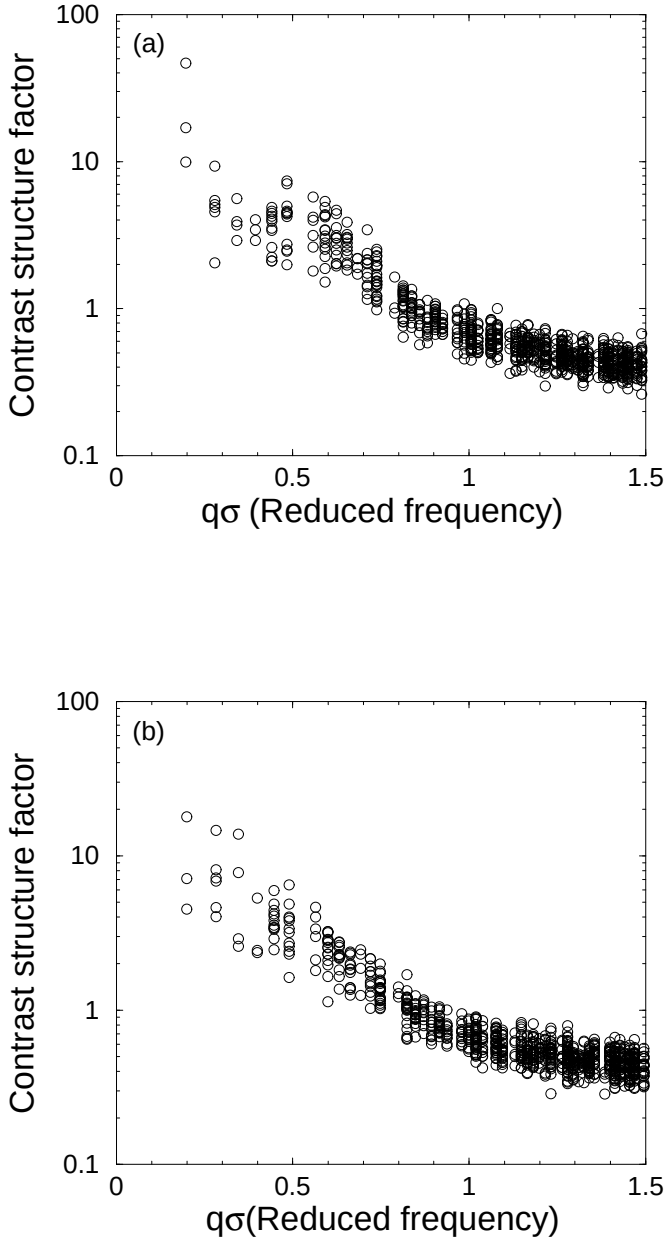

Figure 2: Contrast structure factor for the H_4T_8/solvent system at (a) $\eta = 0.25$ and (b) $\eta = 0.26$ for the same surfactant concentration, temperature, system size and interaction parameters as in figure 1.

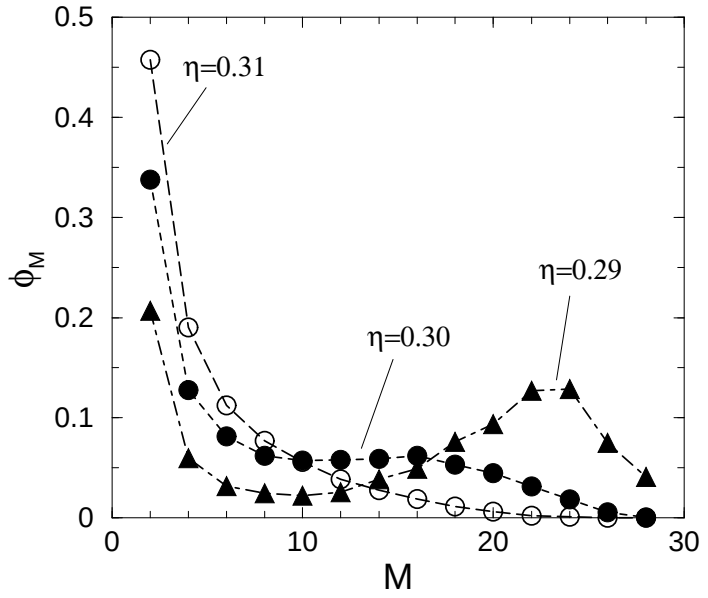

Figure 3: Aggregate (micelle) size distribution at $\eta = 0.29, 0.30, 0.31$ for H_4T_8 at $X_{H_4T_8} = 0.0119$ and $T^* = 1.0$ for the parameter set $\epsilon_{HH} = -1.0$, $\epsilon_{HS} = -0.5$, $\epsilon_{TT} = -0.1$ and $\epsilon_{TS} = -1.0$.

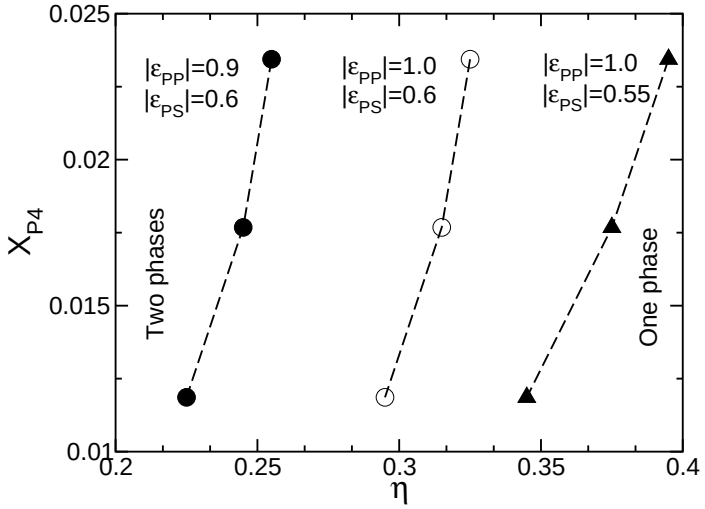

Figure 4: Two phase $\rightarrow$ one phase transition at $T^* = 1.0$ for homopolymer P_4 in the homopolymer mole fraction (X_{P_4}) $-$ packing fraction (η) plane for $(\epsilon_{PP}, \epsilon_{PS}) = (-0.9, -0.6), (-1.0, -0.6)$ and $(-1.0, -0.55)$.

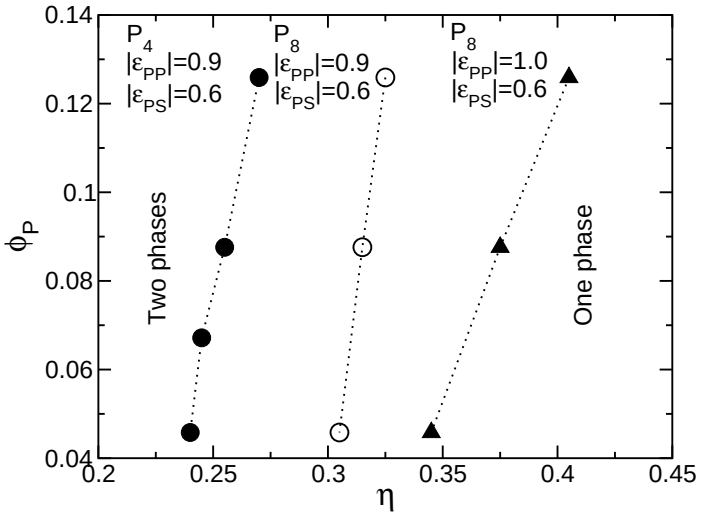

Figure 5: Two phase $\rightarrow$ one phase transition in the homopolymer volume fraction ($\phi_{\rm P}$) $-$ packing fraction (η) plane for homopolymer $\rm P_4$ with $(\epsilon_{\rm PP}, \epsilon_{\rm PS}) = (-0.9, -0.6)$ and for homopolymer $\rm P_8$ with $(\epsilon_{\rm PP}, \epsilon_{\rm PS}) = (-0.9, -0.6)$ and $(-1.0, -0.6)$ at $T^* = 1.0$.

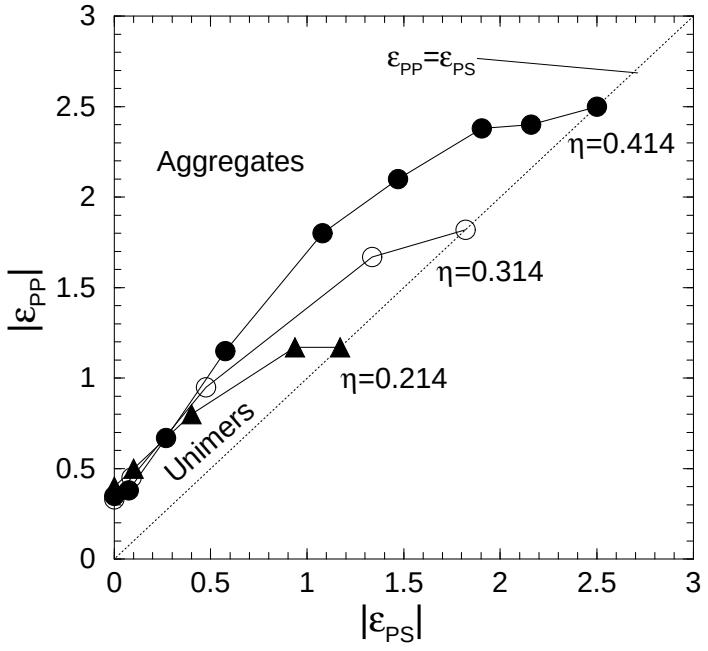

Figure 6: Aggregate $\rightarrow$ unimer transition for homopolymer P_4 in the polymer-polymer attraction ($|\epsilon_{\rm PP}|$) $-$ polymer-solvent attraction ($|\epsilon_{\rm PS}|$) plane at $X_{\rm P_4} = 0.0089$ and $T^* = 1.0$ at $\eta = 0.214, 0.314$ and 0.414.

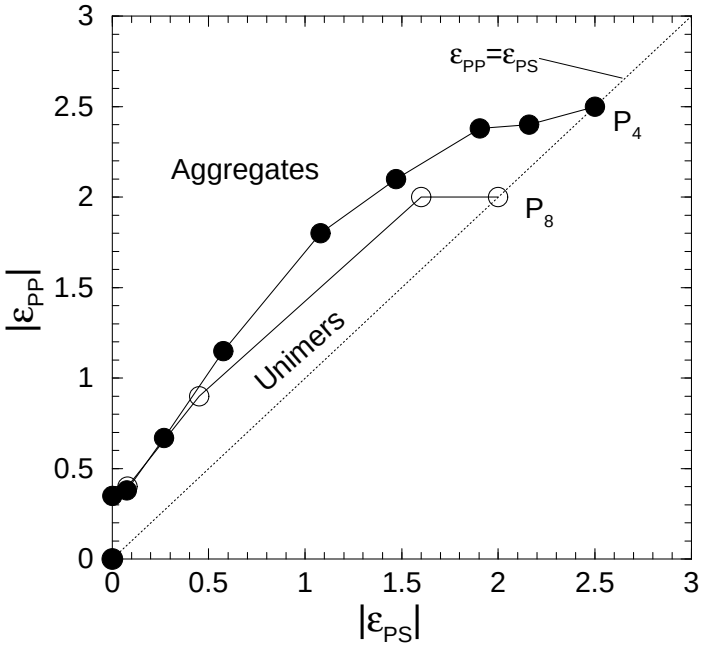

Figure 7: Aggregate $\rightarrow$ unimer transition for homopolymers P_4 and P_8 in the polymer-polymer attraction ($|\epsilon_{\rm PP}|$) $-$ polymer-solvent attraction ($|\epsilon_{\rm PS}|$) plane at homopolymer volume fraction $\phi_{\rm P} = 0.0347$, $\eta = 0.414$ and $T^* = 1.0$.

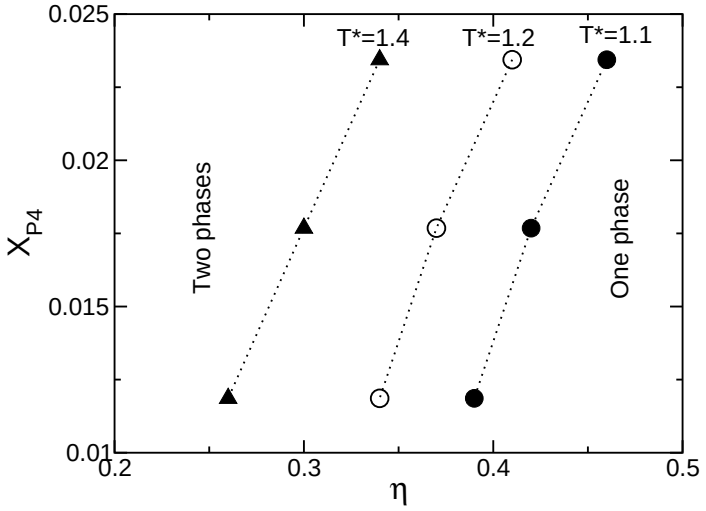

Figure 8: Two phase $\rightarrow$ one phase transition for homopolymer P_4 in the homopolymer mole fraction (X_{P_4}) $-$ packing fraction (η) plane for $(\epsilon_{PP}, \epsilon_{PS}) = (-1.0, -0.5)$ at $T^* = 1.1, 1.2$ and 1.4.

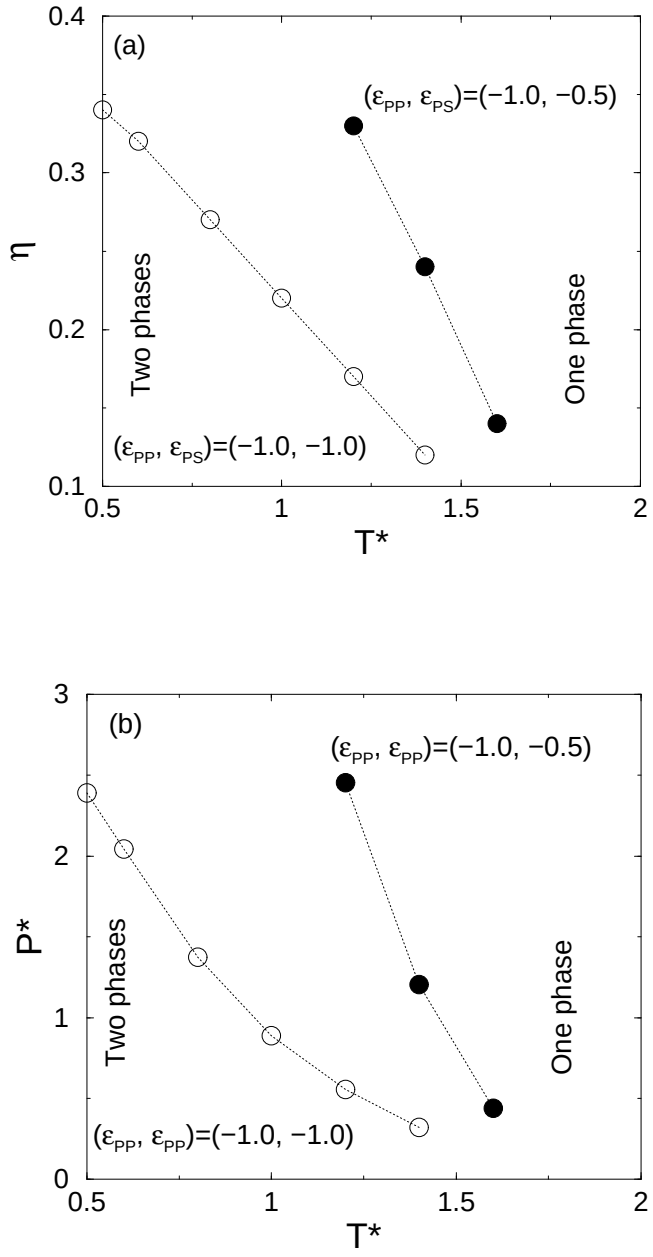

Figure 9: Two phase → one phase transition for homopolymer P_4 in (a) the packing fraction (η) − reduced temperature (T^*) plane, and (b) the reduced pressure (P^*) − reduced temperature (T^*) plane at $X_{P_4} = 0.01768$ for $(\epsilon_{PP}, \epsilon_{PS}) = (-1.0, -0.5)$ and $(-1.0, -1.0)$.

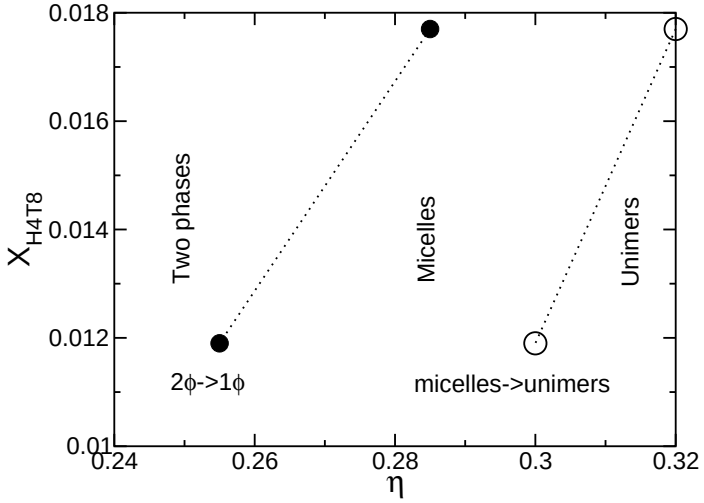

Figure 10: Phase diagram in the surfactant mole fraction ($X_{\mathrm{H_4T_8}}$) $-$ packing fraction (η) plane for surfactant $\mathrm{H_4T_8}$ at $T^* = 1.0$ for the parameter set $\epsilon_{\mathrm{HH}} = -1.0, \epsilon_{\mathrm{HS}} = -0.5$, $\epsilon_{\mathrm{TT}} = -0.1$ and $\epsilon_{\mathrm{TS}} = -1.0$.

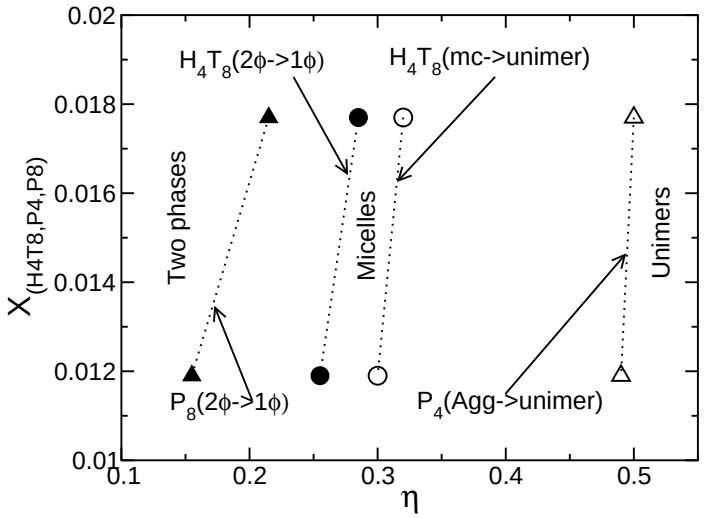

Figure 11: Phase diagram in the polymer mole fraction ($X_{\mathrm{H_4T_8}}$) $-$ packing fraction (η) plane at $T^* = 1.0$ for homopolymer $\mathrm{P_4}$ with $(\epsilon_{\mathrm{PP}}, \epsilon_{\mathrm{PS}}) = (-1.0, -0.5)$, homopolymer $\mathrm{P_8}$ with $(\epsilon_{\mathrm{PP}}, \epsilon_{\mathrm{PS}}) = (-0.1, -1.0)$ and surfactant $\mathrm{H_4T_8}$ with $\epsilon_{\mathrm{HH}} = -1.0$, $\epsilon_{\mathrm{HS}} = -0.5$, $\epsilon_{\mathrm{TT}} = -0.1$ and $\epsilon_{\mathrm{TS}} = -1.0$.

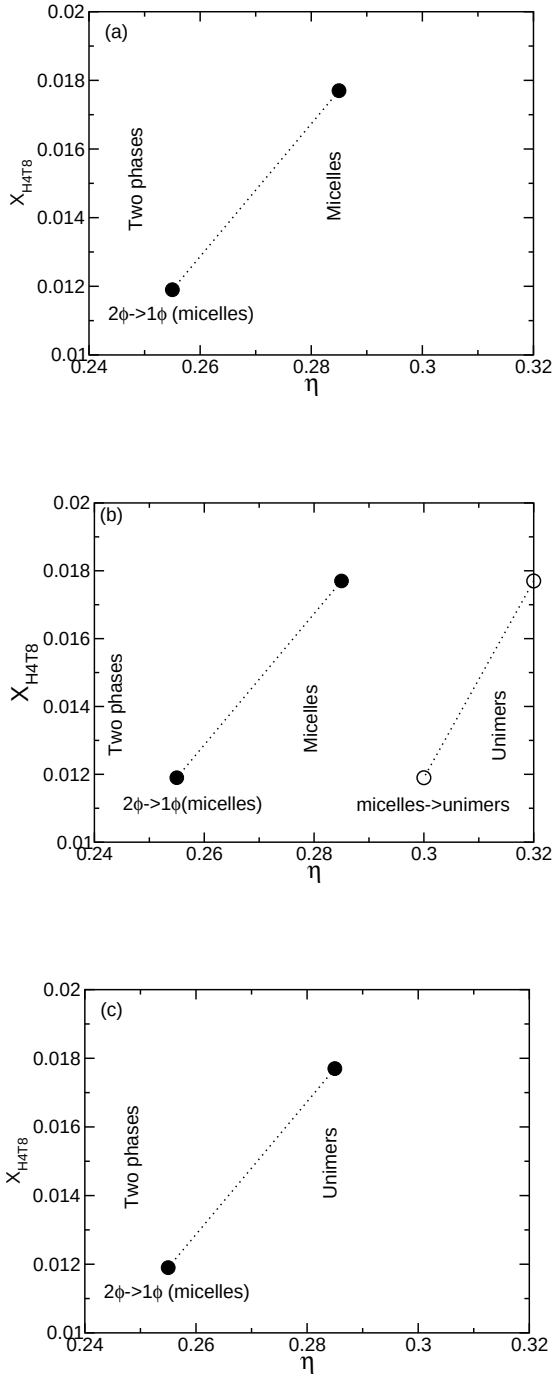

Figure 12: Phase transition in the surfacant mole fraction ($X_{\mathrm{H_4T_8}}$) − packing fraction (η) plane at $T^* = 1.0$ for surfactant $\mathrm{H_4T_8}$ for $\epsilon_{\mathrm{HS}} = (\mathrm{a}) - 0.4, (\mathrm{b}) - 0.5, (\mathrm{c}) - 0.6$ at $\epsilon_{\mathrm{HH}} = -1.0$, $\epsilon_{\mathrm{TT}} = -0.1$, and $\epsilon_{\mathrm{TS}} = -1.0$.

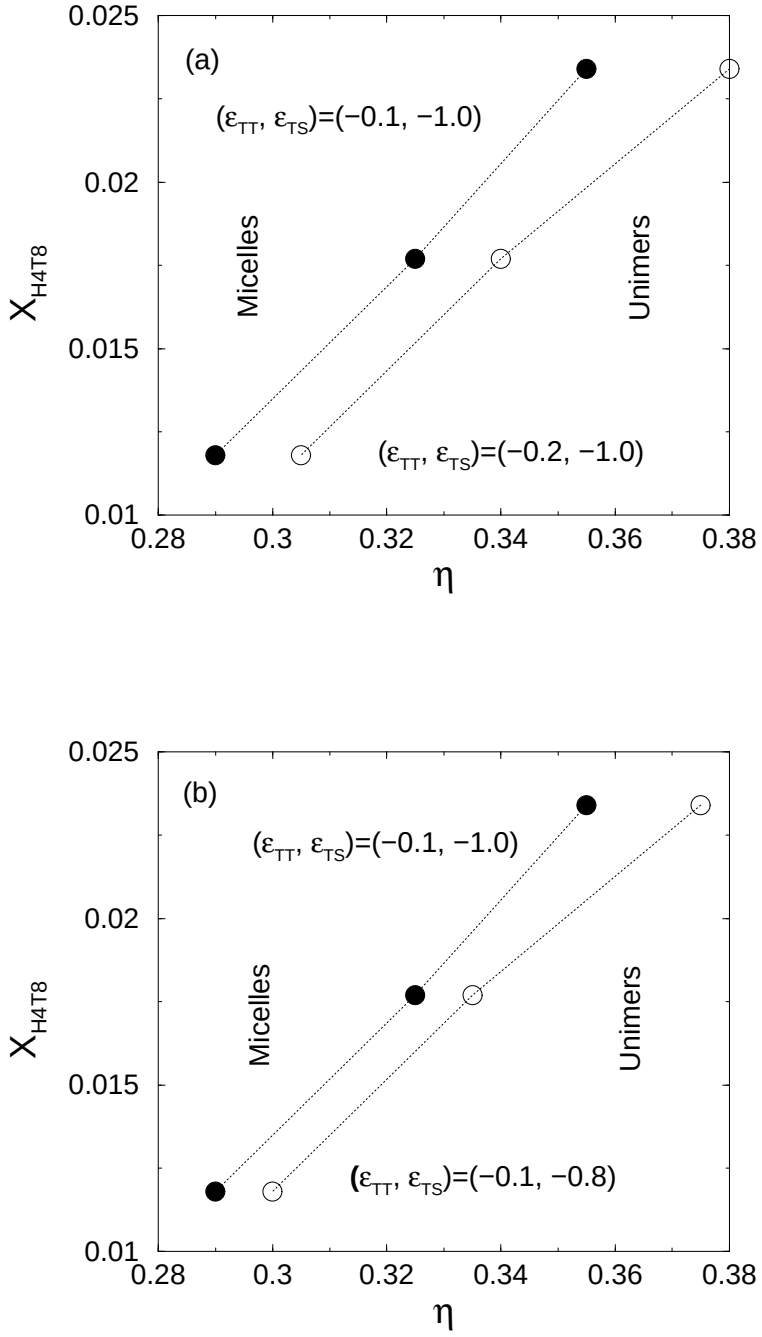

Figure 13: Micelle → unimer transition for surfactant H_4T_8 in the surfactant mole fraction ($X_{H_4T_8}$) − packing fraction (η) plane at $T^* = 1.0$ for $(\epsilon_{TT}, \epsilon_{TS})$ equal to: (a) $(-0.1, -1.0)$ and $(-0.2, -1.0)$ and (b) $(-0.1, -1.0)$ and $(-0.1, -0.8)$, all at $(\epsilon_{HH}, \epsilon_{HS}) = (-1.0, -0.5)$.

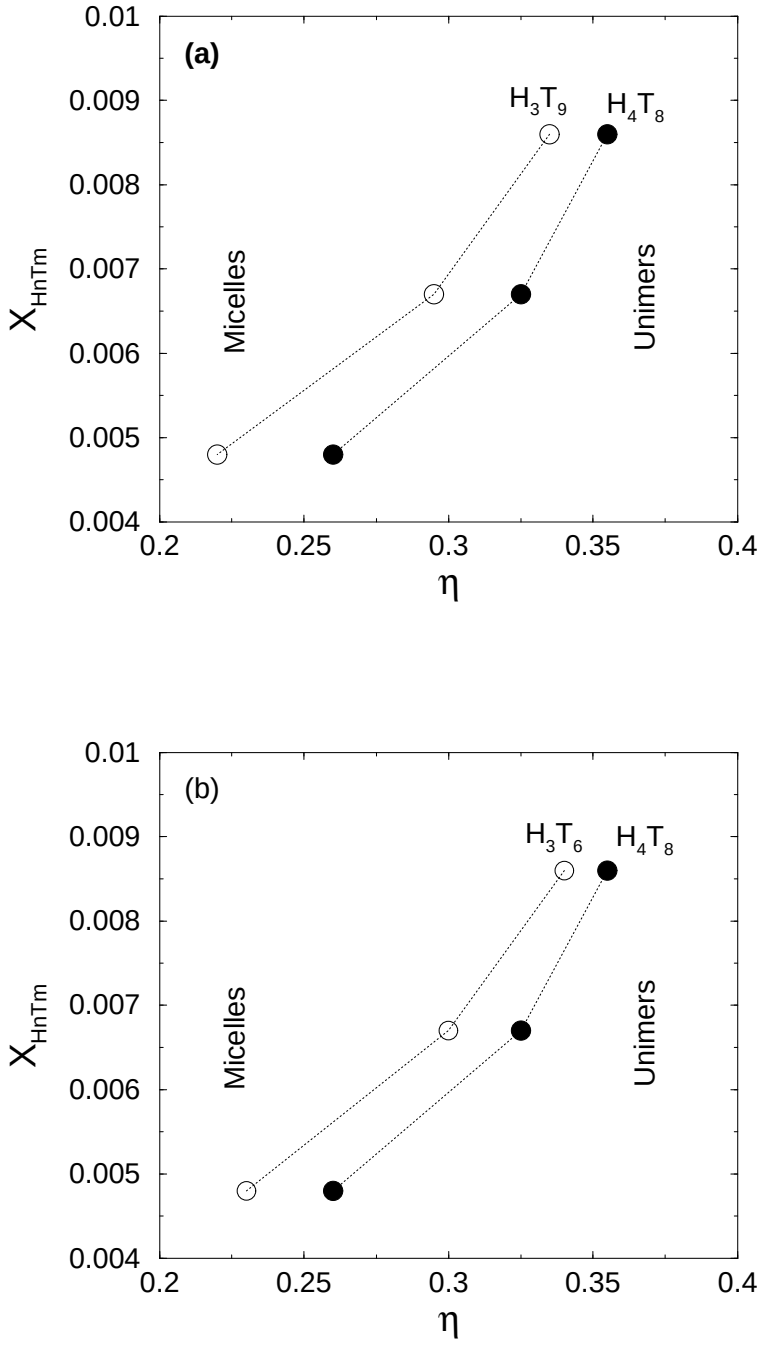

Figure 14: Micelle $\rightarrow$ unimer transition at $T^* = 1.0$ in the surfactant mole fraction ($X_{\mathrm{H_nT_m}}$) $-$ packing fraction (η) plane for surfactants: (a) H_4T_8 and H_3T_9, and (b) H_4T_8 and H_3T_6 at $\epsilon_{\mathrm{HH}} = -1.0, \epsilon_{\mathrm{HS}} = -0.5, \epsilon_{\mathrm{TT}} = -0.1$ and $\epsilon_{\mathrm{TS}} = -1.0$.

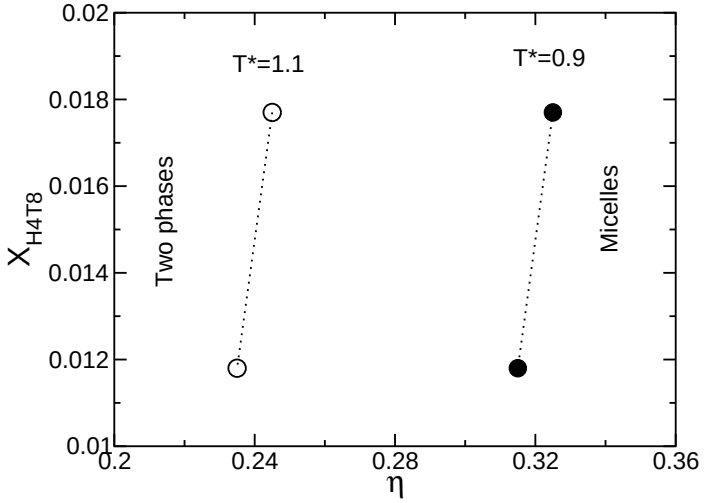

Figure 15: Phase diagram for surfactant H_4T_8 in the surfactant mole fraction ($X_{H_4T_8}$) $-$ packing fraction (η) plane at $T^* = 0.9$ and 1.1 for $\epsilon_{HH} = -1.0, \epsilon_{HS} = -0.5, \epsilon_{TT} = -0.1$ and $\epsilon_{TS} = -1.0$.

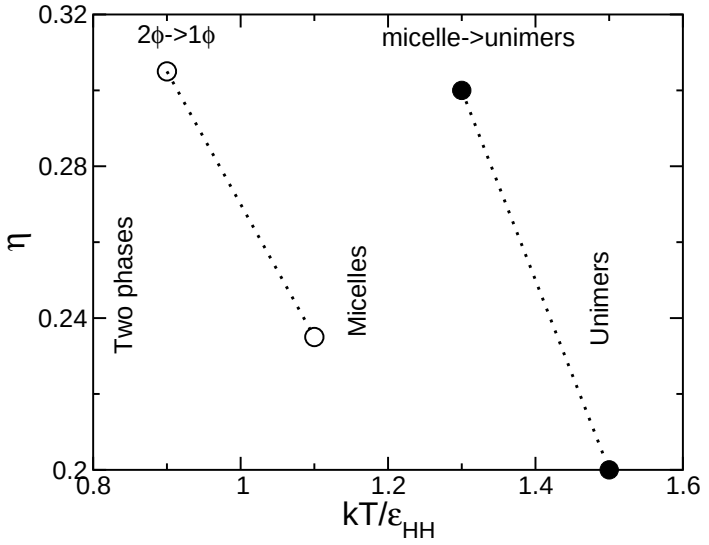

Figure 16: Phase diagram for H_4T_8 at $X_{H_4T_8} = 0.0177$ in the packing fraction (η) $-$ reduced temperature (T^*) plane for $\epsilon_{HH} = -1.0, \epsilon_{HS} = -0.5$, $\epsilon_{TT} = -0.1$ and $\epsilon_{TS} = -1.0$.

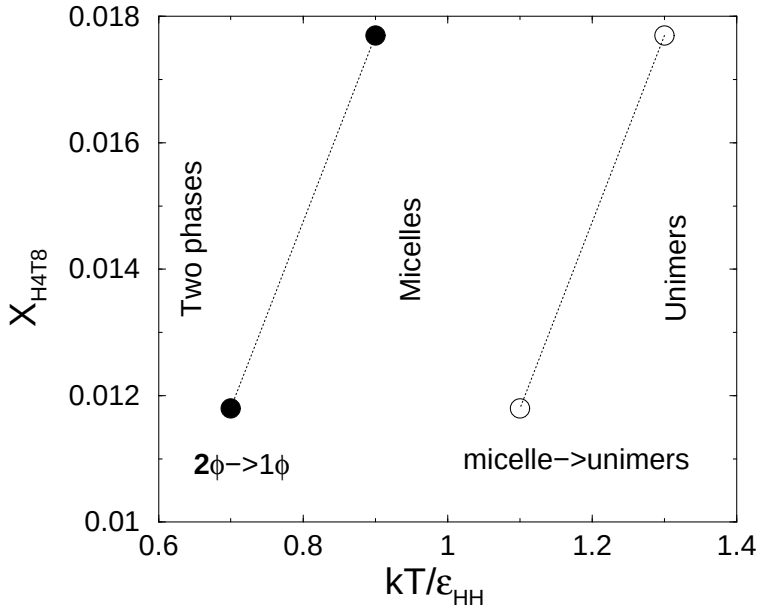

Figure 17: Phase diagram for surfactant H_4T_8 in the surfactant mole fraction ($X_{H_4T_8}$) − reduced temperature (T^*) plane at $\eta = 0.30$ for $\epsilon_{HH} = -1.0, \epsilon_{HS} = -0.5$, $\epsilon_{TT} = -0.1$ and $\epsilon_{TS} = -1.0$.